PHYSICAL REVIEW B VOLUME 7, NUMBER 6 15 MARCH 1973

Quantum Aspects and Electrodynamics of High-Frequency Cyclotron Resonances in Bismuth

U. Strom,* Avid Kamgar, and J. F. Koch
University of Maryland, College Park, Maryland 20742
(Received 2 October 1972)

We present a series of measurements on various aspects of cyclotron resonance in Bi at far-infrared laser frequencies (890.7, 964.3, 1539.5, and 2526.6 GHz). The experiments make use of a spectrometer where the sample forms one plate of a TEM-mode strip transmission line. We observe subharmonics of cyclotron resonance which appear split into a number of distinct resonance lines, each due to a particular transition between Landau levels of the nonparabolic conduction band of Bi. From the line positions for the binary-axis low-mass resonance we determine the band parameters $E_g = 13.0 \pm 2$ meV and $m^*_c = (0.00170 \pm 0.00025) m_0$. The temperature dependence of the amplitudes of the resonance lines gives $E_F = 29.7 \pm 0.5$ meV. We observe the amplitude decay of successive subharmonics of the resonance and show that the amplitude decreases with subharmonic number n approximately as $(R/\delta)^{2n-2}$ for the binary-axis signal. In addition to cyclotron resonance, we observe and identify various impedance anomalies as due to cyclotron-wave propagation. Finally, we present some evidence for an energy-dependent relaxation time in Bi, from the observation that cyclotron-resonance linewidths are related to the energy separation of Landau level and Fermi energy.

I. INTRODUCTION

Cyclotron-resonance (CR) studies in the semimetal Bi are a classic experiment for which a large body of scientific literature has accumulated over the years. The published work divides readily into two categories according to the range of experimental frequencies employed in the investigation. On the one hand, there are the conventional microwave-frequency (10–100 GHz) investigations, i.e., Azbél–Kaner cyclotron resonance (AKCR), which measures the properties of electrons at the Fermi energy E_F. Both the microwave energy $\hbar\omega$ and thermal energy kT at low temperatures (~4 °K) are very much less than E_F. Thus microwave CR is a classical effect in which resonance corresponds to transitions between many sets of Landau levels within $\pm kT$ of E_F. As is well known, the electron energy bands of Bi are such that the effective cyclotron mass m_c^* is a function of energy. However, since for AKCR all transitions occur in the immediate vicinity of E_F, all electrons on the ellipsoidally shaped Fermi surface (FS) have the same resonance frequency and contribute to microwave CR. The authoritative work on cyclotron effective masses in Bi, as well as on cyclotron waves (CW) and other electromagnetic modes, is due to Khaikin and his co-workers.[1–3]

At the other end of the frequency spectrum are the infrared interband magnetoreflection experiments at frequencies above 10 000 GHz.[4] For these $\hbar\omega$ is larger than E_F and much larger than kT. Resonant transitions from individual Landau levels in the valence band to those in the conduction band are observed at high magnetic field values. Under appropriate conditions an intraband CR fundamental, for which the change in Landau level number is unity, is observed in magnetoreflection. These experiments have provided the essential band-structure information in Bi, but they are relatively insensitive to the precise value of E_F. Generally the magnetoreflection data appear as rather broad sinusoidal oscillations of the reflectivity, as compared to the sharp spikelike resonances that are observed in microwave-frequency CR under high-$\omega\tau$ conditions.

The present CR experiments at the far-infrared laser frequencies of 890.7, 964.3, 1539.5, and 2526.6 GHz scan a frequency range intermediate to the previous microwave CR and magnetoreflection experiments and, so to say, bridge the gap between them. In this experiment we observe the intraband transitions between the levels above the gap. In Fig. 1 we have shown the Landau levels and characteristic transitions for the three types of experiments. As expected, our data contain features of both the classical AKCR and magnetoreflection experiments. We find the subharmonic sequence of peaks as in AKCR, although these are rapidly attenuated and accompanied by strong CW effects. We also find that these subharmonics are split into multiplets of individual peaks, each due to a single distinct quantum transition between a pair of Landau levels in the nonparabolic conduction band of Bi. We find that, in general, the nth subharmonic of CR consists of n lines, whose positions measure the band parameters and whose relative amplitudes depend on the position of the Landau level relative to the Fermi level. Thus a single experiment measures both the band parameters and E_F. As in the case of magnetoreflection our experiments select essentially the central, k_H

= 0, transitions between Landau levels.

The far-infrared frequencies for our experiments are also significant in that they are comparable to zone-boundary acoustic- and optical-phonon frequencies in Bi. One might expect that some evidence for the electron-phonon interaction appears in the form of a frequency-dependent cyclotron mass, or a frequency-dependent electronic lifetime similar to those found in other metals by Goy and Castaing.[5] There is a definite indication of an energy-dependent electronic lifetime in Bi from our experiments. The cyclotron mass which we determine appears just slightly larger than the microwave value, but such possible mass shift has to be viewed with caution because of comparable experimental uncertainties.

The surface impedance in the present far-infrared experiments is dominated by various propagating electromagnetic modes and resonances—dielectric anomalies, hybrid resonances, and various modes of Alfven waves, as well as CW waves. Such collective modes have been explored in a number of microwave-frequency experiments over the years,[2,6] and by and large the microwave results seem to carry over to high frequencies. The same dielectric anomalies, hybrid resonances, and CW impedance anomalies are observed, but an interesting departure from their expected frequency scaling becomes apparent above 1000 GHz as exemplified by our study of the CW anomaly. The emphasis of the present work has been on CR transitions, and the CW spectrum which is intimately tied to CR. A consequence of this effort to observe and interpret high-frequency CR has been to restrict us to the low-mass electron resonances at the binary and bisectrix axes of Bi. The high-mass resonances in these and other directions are largely obscured and modified by propagating wave effects and could not readily be interpreted as CR.

Section II gives relevant experimental details of the rather novel spectrometer that we have devised for this work. Section III deals with our observations as they affect the electrodynamics of CR at high frequencies. Section IV explores the quantum aspects and splitting of subharmonic peaks to derive an accurate set of band parameters and a value for E_F. This is followed in Sec. V by some remarks on electronic lifetimes. Section VI presents concluding remarks and observations.

II. EXPERIMENTAL NOTES

The far-infrared frequencies used in the present experiment are in an unconventional range of frequencies for studying the surface impedance of metals. With the development of gas-laser sources and sensitive radiation detectors this region of the spectrum has recently become more accessible. Because absorption of an electromagnetic wave at a metal surface is generally weak, for such studies a device is required which permits multiple reflections. Such a device may be of the resonant type as the confocal resonator used by Allen,[7] or the nonresonant-strip transmission-line arrangement as used in this experiment. In the following we will briefly describe the important features of our laser–transmission-line spectrometer.

The laser is a conventional design with the semiconfocal arrangement of one flat and one spherical mirror whose radius is on the order of, but larger than, the mirror separation. The electrodes are

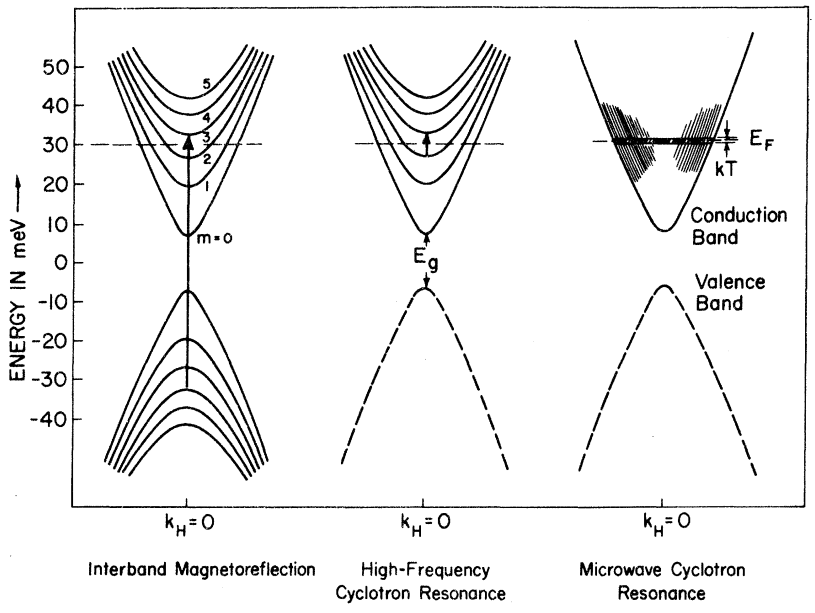

FIG. 1. Landau levels for electrons in Bi. Resonance transitions as in interband magnetoreflection and high-frequency cyclotron resonance are indicated at $k_H = 0$. In microwave CR, transitions extend over the entire range of k_H and throughout an energy width of order kT.

made of copper and are in the shape of hollow cylinders. Support rods of Invar metal are used to keep the mirror separation fixed against the thermal expansion of the glass cavity. The relevant dimensions of the system are as follows: laser-tube diameter, 0.10 m; mirror separation, 3.40 m; mirror radius, 7.00 m; electrode separation, 2.90 m.

We have operated the laser at the two dominant frequencies of the cyanide gas, 890.7 and 964.3 GHz, using a gas mixture of methane and nitrogen. The additional frequencies 1539.5 and 2526.6 GHz are obtained from deuterated acetonitrile and water vapor, respectively. The power output at cyanide frequencies is of the order of a few milliwatts, with stability of about 0.03% when using a 1-sec time constant in the detector circuit. At the other two frequencies we have somewhat less power and less stability.

The essential element of the laser spectrometer is a transverse-electromagnetic (TEM)-mode strip transmission line which is a modified version of the transmission-line geometry originally developed by Drew and Sievers.[8] It is made of two parallel plates, one of which is the sample under investigation and the other a polished copper plate. Its dimensions are about 1×1 cm and the spacing is about 25 μm. The spacing is therefore much less than the wavelength of the far-infrared radiation (100–300 μm). Consequently, only a TEM mode is propagated. For such a mode the current $\vec{J}$ induced in the walls will flow parallel to the propagation direction of the radiation. With proper choice of the direction of the magnetic field $\vec{H}$ both $\vec{J}\parallel\vec{H}$ and $\vec{J}\perp\vec{H}$ configurations can be achieved. The damping of the TEM wave is a consequence of the finite surface resistance of the walls. For a radiation power P_0 entering a transmission line of length L and spacing d, the transmitted power is

$$P(H)=P_0e^{-R(H)L/Z_0d}, \tag{1}$$

where Z_0 is the impedance of free space and R is the real part of the surface impedance of the two plates and depends on the magnetic field. The quantities measured in the experiment are dP/dH and P, while the quantity of interest is the field derivative of surface resistance which according to Eq. (1) is given by $dR/dH=(\text{const})\,(1/P)\,(dP/dH)$. In the experiments we measure both P and dP/dH and construct dR/dH according to this relation.

From the approximately known sensitivity of our bolometer detector circuit ($\sim10^4$ V/W) an estimate can be made of the sensitivity of the spectrometer. The laser output is about 10^{-3} W. The losses in the cones used to channel the radiation into the transmission line are such that the power inside the transmission line is only about 10^{-5} W. The measured noise level of the bolometer corresponds to a power level of $\sim10^{-10}$ W. Consequently, the fractional change in power level that can be detected is $\Delta P/P\simeq10^{-5}$. The corresponding fractional change in resistance

$$\Delta R/R=-(Z_0d/RL)\,(\Delta P/P) \tag{2}$$

depends on the transmission-line parameters. For the dimensions quoted above, $Z_0d/RL\sim1$–10 for a semimetal. Thus typical changes in the surface resistance of $\Delta R/R\simeq10^{-4}$–10^{-5} can be measured.

The cryostat and the light-pipe arrangement, as shown in the sketch of Fig. 2, is a modified version of the system used in earlier work.[9] It is a more practical design in which we place both the sample and the detector, and also the magnet when we use the superconducting coil, in the same He Dewar. The laser radiation is guided through $\frac{1}{2}$-in. brass light pipe and is channeled by a long cone to the transmission line which is placed at the center of the magnet. A dc magnetic field is applied parallel to the surface of the sample and either parallel or perpendicular to the direction of propagation. In the case of parallel polarization a superconducting solenoid is employed and for the perpendicular polarization we use a conventional iron magnet. The magnetic field is modulated at some low frequency compatible with the detector time constant. The transmitted power is detected with a GE bolometer placed at the bottom of the light pipe. The whole transmission line assembly and the detector are in vacuum. The output of the

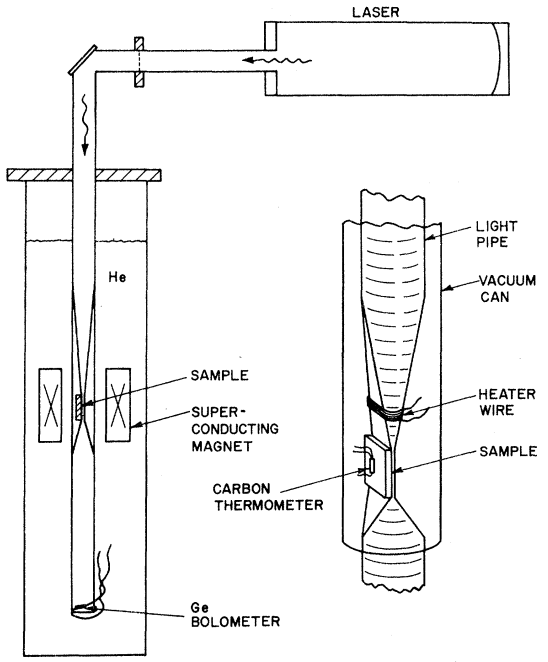

FIG. 2. Experimental arrangement of the laser spectrometer.

bolometer is detected in a lock-in amplifier which is tuned to the modulation frequency of the magnet, and the output of the phase-sensitive detector is a measure of dP/dH. To measure the total transmitted power $P(H)$ we chop the laser radiation at a low frequency and detect the signal at this frequency as a function of the applied field.

The temperature-dependence studies employ a heater element to raise the sample temperature above that of the helium bath. The entire transmission-line assembly is placed inside an evacuated stainless-steel can. For measuring the temperature we use a calibrated carbon thermometer which is glued to the back surface of the sample.

Samples are grown from 99.9999%-pure Cominco Bi boules. The desired amount of Bi is placed in high-purity graphite mold and melted to form rectangular slabs of the approximate dimensions of $3\times15\times40$ mm. It is then seeded in the desired plane and direction and grown in vacuum by the Bridgman technique. The accuracy of the plane and direction is checked with x-ray Laue photographs. All samples are acid lapped on a Teflon cloth and chemically polished to obtain smooth and flat surfaces.

III. ELECTRODYNAMICS OF HIGH-FREQUENCY CYCLOTRON RESONANCE

In this section we make some remarks and observations on the electrodynamics of high-frequency CR experiments in Bi. Our perspective is to consider the conventional AKCR as the expected norm and to explore the various modifications and changes that occur with increasing frequency. The discussion will be centered on three specific themes—the amplitude decay of successive subharmonics, the amplitude dependence on the polarization because of Hall-effect screening of CR, and finally, the strong CW effects that accompany high-frequency CR.

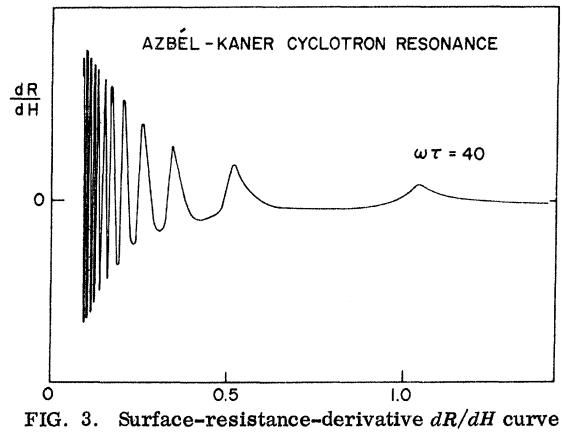

FIG. 3. Surface-resistance-derivative dR/dH curve for Azbél–Kaner cyclotron resonance calculated for $\omega\tau=40$.

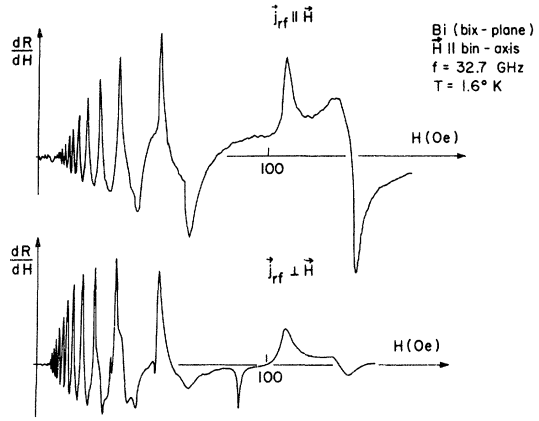

FIG. 4. Microwave-frequency CR in Bi for currents aligned parallel and perpendicular to the magnetic field.

A. Amplitude Decay of Subharmonics

For the low-mass binary-axis resonance the cyclotron radius R_c is related to the magnetic field approximately as $R_c \approx 4\times10^{-2}/[H(\text{Oe})]$ cm. The measured radio-frequency skin depth δ is typically 0.7×10^{-4} cm at 24 GHz.[10] Conventional AKCR, with its requirement of $R \gg \delta$ would be observed only at very low GHz frequencies. For example, at 1 GHz the fundamental resonance occurs at about 4 Oe $[m_c^*(E_F)=0.0093m_0]$ and the cyclotron radius at the fundamental is $R \approx 1\times10^{-2}$ cm. The skin depth would be $\delta \approx 2\times10^{-4}$ cm. Thus $R/\delta \approx 50$, and one expects to observe a typical AKCR spectrum with a conventional subharmonic sequence of peaks as in the theoretical curve of Fig. 3. This curve is drawn for $\omega\tau=40$ and for the limiting case $R \gg \delta$. Because $\frac{2}{3}$ of all the electrons on the FS participate in the resonance, the Bi signal should approximate the case, originally assumed by Azbél and Kaner,[11] where all carriers resonate simultaneously.

Even at conventional microwave frequencies (10–100 GHz) one observes for Bi a spectrum different from Fig. 3 with respect to the amplitude decay of subharmonics. An example of this is the experimental curve of Fig. 4 at 32.7 GHz. Scaling R and δ to the frequency employed in Fig. 4 we find $R/\delta \approx 5$, so that the $R \gg \delta$ as required in Azbél–Kaner theory is not satisfied. The essential difference is that the transit time of an electron through the skin layer is no longer negligibly small compared to the rf period, and retardation effects of the type discussed in several recent publications[12–14] apply. Azbél–Kaner theory predicts an amplitude decay with increasing subharmonic number n as $dR/dH \propto n^2 e^{-2\pi n/\omega\tau}$. Drew[12,14] has shown, when retardation applies, the electron scattering rate $(1/\tau)$ is to be replaced by $(1/\tau)_{eff}=\gamma_{eff}$ such that

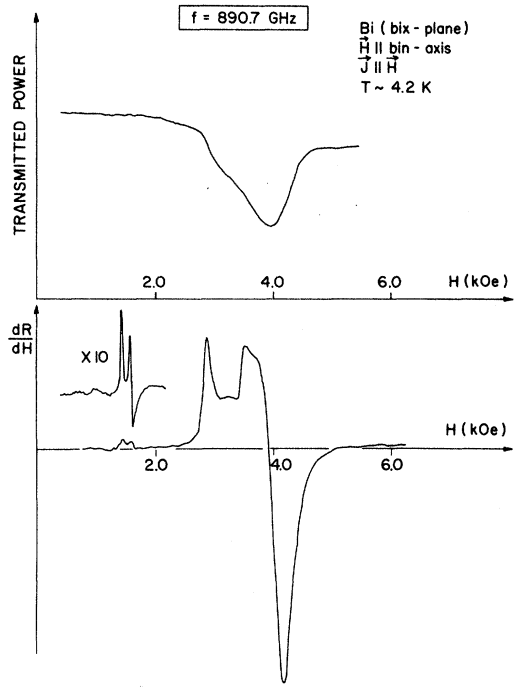

FIG. 5. Transmitted power and dR/dH curves at 890.7 GHz.

$$\gamma_{eff} \approx 1/\tau + \omega\delta/2\pi R \,. \tag{3}$$

The second term represents damping due to the finite transit time of electrons through the skin layer. The expression as written applies to a circular orbit. From a plot of $\ln(\text{amplitude}/n^2)$ vs n for the case of perpendicular polarization we find the value $\gamma_{eff} \approx 1.5\times10^{10}$ sec^{-1}. The linewidth and line shape of the low-order resonances ($n=1$, 2) in Fig. 4 indicate (compare with Fig. 3) a $\omega\tau \approx 40$ or a $1/\tau \approx 0.5\times10^{10}$ sec^{-1}. Thus the observed amplitude decay gives a value of $\omega\delta/2\pi R$ on the order of 1×10^{10} sec^{-1}. Using the previously estimated $R/\delta \approx 5$ at 32.7 GHz we expect $\omega\delta/2\pi R \approx 0.7\times10^{10}$ sec^{-1}. We conclude that the amplitude decay of the Bi CR spectrum in low fields is in large measure due to the retardation effect.

We next consider the retardation effect as it applies at submillimeter wavelengths. Figures 5–8 show in succession the binary-axis low-mass spectrum at frequencies 890.7, 964.3, 1539.5, and 2526.6 GHz. The data are for a bisectrix-plane sample and for currents aligned parallel to the applied field. The upper curve in each case represents the power transmitted, and the lower spectrum is the surface-resistance derivative. The fundamental CR is identifiable as a sharp positive dR/dH peak. Second ($n=2$), and sometimes third ($n=3$), subharmonics appear as multiplets of split peaks with greatly reduced amplitudes. In a previous publication[9] we have explained the multiplet structure as due to distinct quantum transitions between Landau levels and in Sec. IV we shall explore it in more detail. For the present our in-

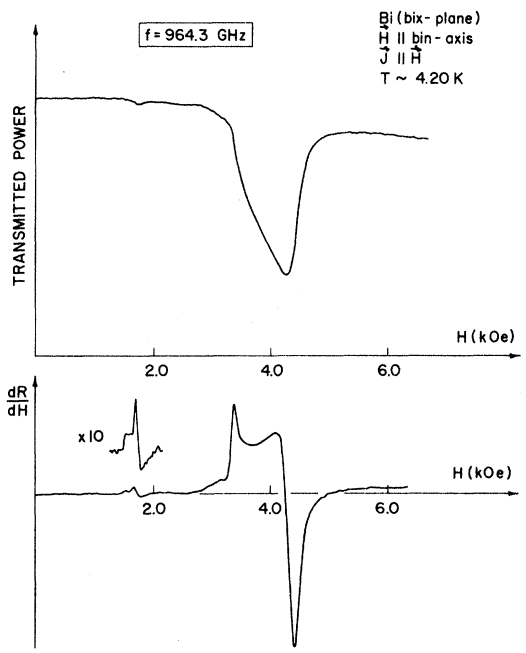

FIG. 6. Transmitted power and dR/dH curves at 964.3 GHz.

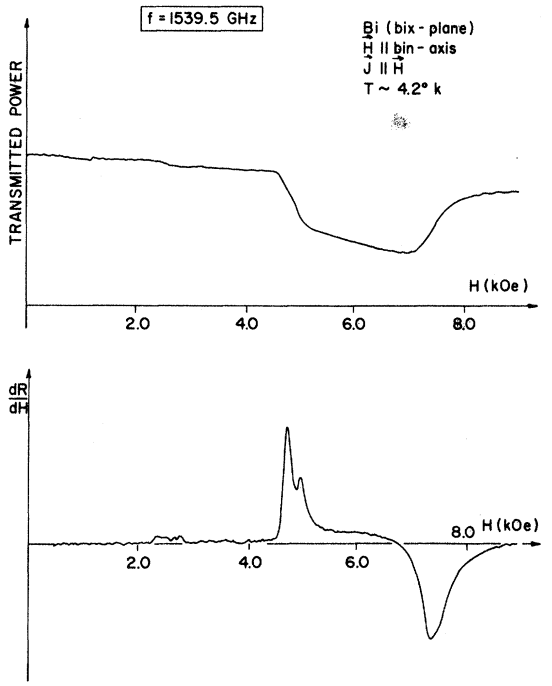

FIG. 7. Transmitted power and dR/dH curves at 1539.5 GHz.

terest is to account for the rapid amplitude decay evident in the curves of Figs. 5–8.

Drew's treatment of retardation does not apply here because the high-frequency data are taken under conditions where $R < \delta$. In recent work[15] Meierovich considers CR for the case of arbitrary R/δ. His expression for the conductivity in the limit $R/\delta < 1$ predicts a rapid amplitude decay with increasing subharmonic number n in terms of a power law involving $(R/\delta)^{2n}$. However, the theory is not immediately applicable to the present measurements without modifications and some additional assumptions. First, Meierovich assumes spherical FS geometry and currents parallel to the applied field. Instead, the observed resonance is due to central tilted orbits on a cylindrical section of the FS. Second, he treats the impedance changes in the large signal limit while we believe that at these high frequencies the small signal limit, as discussed by Chambers,[16] is a better approximation to the experimental conditions. This is because in contrast with the microwave data in Bi, the high-frequency signal is due to only a narrow band of orbits about the central cross section of the ellipsoid. In order to calculate the impedance in the limit where the resonant contribution to σ is due to only a small fraction of electrons, we follow the formulation developed by Prange and Nee[17] to write

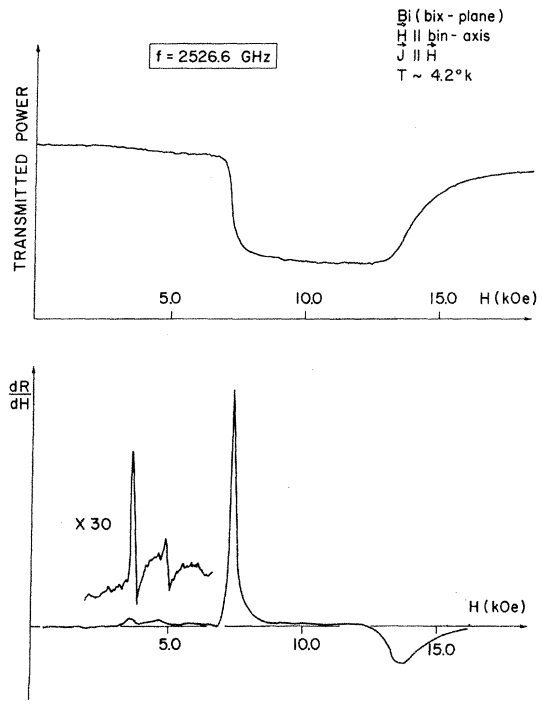

FIG. 8. Transmitted power and dR/dH curves at 2526.6 GHz.

$$-\frac{\Delta Z(H)}{Z^2(0)} \approx \frac{1}{E(0)^2}\int_0^\infty J_{\rm res}(z, H)E(z)\,dz\,, \tag{4}$$

where the change of impedance $\Delta Z(H)$ is expressed as an integral of the electrical current due to a supposedly small group of resonant electrons moving in an assumed reasonable electric field $E(z)$ in the surface region. For present purposes we take the latter in the form $E(0)e^{-z/\delta}$, where δ is the complex skin depth. We express the current associated with the nth subharmonic of CR in terms of the Fourier integral

$$J_{{\rm res},n}(z) = \int_{-\infty}^{\infty} \sigma_n(k)E(k)e^{ikz}\,dk\,, \tag{5}$$

with the understanding that $\sigma_n(k)$ represents the Fourier component of the conductivity due to the small number of resonant electrons.

To derive $\sigma_n(k)$ we follow the work of Meierovich[15] but applied to the case of a tilted orbit on a cylindrical section of the FS and current directed along H. This expression for σ is formally identical with that for a plane orbit and perpendicular polarization. Using the notation as in Ref. 15 we write σ in the form [compare to Eq. (3.1) in Ref. 15]

$$\sigma(k) \propto \beta\int_0^{2\pi} dz \int_0^\infty e^{-2\beta x}\sin(z-x)\sin(z+x) \times\cos(\alpha\cos z\sin x)\,dx\,, \tag{6}$$

where $\alpha = 2kR_c$ and $\beta = i(\omega/\omega_c) + 1/\omega_c\tau$. Here R_c is the field-dependent cyclotron radius. At the nth subharmonic resonance, $R_c = nR$, where R is radius at the fundamental resonance. Following the mathematical procedure of Ref. 15, we obtain

$$\sigma(k) \propto \left(\lambda_0(\alpha) + 2\sum_{\nu=1}^{\infty}\lambda_\nu(\alpha)\right)\,, \tag{7}$$

where

$$\lambda_\nu(\alpha) = \int_0^{2\pi} dz\, J_{2\nu}(\alpha\cos z)\left(-\frac{2\beta^2}{\beta^2+\nu^2}\cos 2z + \frac{\beta^2}{\beta^2+(\nu+1)^2} + \frac{\beta^2}{\beta^2+(\nu-1)^2}\right)\,. \tag{8}$$

If we assume $\omega_c\tau \gg 1$ and concentrate on the vicinity of the nth subharmonic, where $\beta \approx in$, it is seen that only terms with $\nu = n$, $n \pm 1$ are important. Furthermore, α is a parameter which for the most important k values is equal to the ratio of the diameter of the electron orbit to the skin depth. Hence it is a small quantity in our limit of high frequencies. This allows us to expand the Bessel functions as $J_n(z) \approx (\frac{1}{2}z)^n/n!$, and retain only the lowest-order term in α. This is the $\nu = n - 1$ term. Thus the important contribution to the resonant conductivity at the nth subharmonic is

$$\sigma_n(k) \propto \frac{\beta^2}{\beta^2+n^2}\,\frac{n^{2n}}{2^{2n}(n!)^2}\,(kR)^{2n-2}\,. \tag{9}$$

TABLE I. Amplitude ratios and R/δ values for $\vec{H}\parallel$ binary axis; $\vec{J}_{rf}\perp\vec{H}$; $T\cong 4.2$ °K. A_1, A_2, and A_3 are the dR/dH amplitudes of a single line in the first, second, and third subharmonics, respectively. The values for R/δ have been calculated using the relation in Eq. (11).

Frequency (GHz)	A_1/A_2	A_2/A_3	R/δ
890.7	10 ± 1	18 ± 5	0.32
1539.5	20 ± 5		0.22
2526.6	45 ± 5		0.15

This expression for $\sigma_n(k)$ is essentially the same as that derived by Kaner and Skobov[18] [Eq. (335) in Ref. 18]. From Eq. (5) we now express the current as

$$J_{res,n}(z)\propto\frac{\beta^2}{\beta^2+n^2}\,\frac{n^{2n}}{2^{2n}(n!)^2}\,R^{2n-2}\times\int_{-\infty}^{\infty}k^{2n-2}\,\frac{2\delta}{(k\delta)^2+1}\,e^{ikz}\,dk\,. \quad (10)$$

We have substituted the Fourier spectrum of the electric field as $E(k)=2\delta/(k^2\delta^2+1)$, corresponding to the assumed form of the spatial dependence. We finally convert the integral to a contour integral in the complex k plane and evaluate the residue at the pole $k=+1/\delta$ to find the change of impedance at the nth subharmonic as proportional to

$$\Delta Z_n\propto\frac{n^{2n}}{2^{2n}(n!)^2}\left(\frac{R}{\delta}\right)^{2n-2}. \quad (11)$$

Thus successive subharmonics decay in amplitude as a geometric progression in $(R/\delta)^2$ with some multiplicative factors involving n. We remind the reader that in Eq. (11), R is the cyclotron radius at the fundamental resonance and δ is the magnitude of skin depth.

In comparing this decay law to the experiments, one encounters some difficulties. The fundamental (possibly also the subharmonics) is distorted due to the presence of propagating-wave effects, which appear as structure adjacent to the resonances. Quantum effects, such as the occupation probability of Landau levels, are expected to influence resonance amplitude. Also, one may question how well a classical circular orbit, as used in the conductivity calculation, represents the low-index-number Landau levels between which the transitions occur. Keeping these limitations in mind, we can only make a qualitative check on the amplitude decay law as derived above. For that purpose we consider the change of surface resistance at the nth subharmonic ΔR_n as the product of peak amplitude and linewidth. Linewidth reduces by a factor n with increasing subharmonic number, while there are, in general, n peaks in the multiplet whose contributions must be summed. These two factors cancel allowing us to compare derivative amplitudes of a single peak of each subharmonic. We use only peak amplitudes where the transition is allowed by the same quantum statistics factors (see Sec. IV for the temperature dependence of amplitudes). Table I gives the numerical comparison of peak amplitudes and derives a value of R/δ at 890.7, 1539.5, and 2526.6 GHz. We compare the R/δ values in Table I with an estimate based on scaling R and δ from microwave frequency. Assuming that $\delta\propto\omega^{-1/3}$ and $R\propto 1/\omega$, we would find $R/\delta\approx 0.56$, 0.39, and 0.28 at the three frequencies listed in the table. Neither the ω scaling for the skin depth, nor the scaling assumed for R in this quantum region, are expected to be valid. Consequently, the discrepancy between experimental and estimated R/δ should not come as a surprise.

B. Polarization Dependence of Amplitudes

The microwave data of Fig. 4 suggest a curious amplitude dependence of the fundamental resonance on the polarization of the rf current. In the perpendicular mode the fundamental peak is notably smaller relative to the second- and higher-order subharmonics when compared to the parallel polarization data. Keeping in mind that the ellipsoids are tilted 30° with respect to the binary axis, the parallel-polarization geometry is a case of tilted-orbit CR. From the point of view of AKCR one should have expected similar spectra. The difference in the relative amplitude of the fundamental with polarization becomes even more pronounced at higher frequencies and decreasing R/δ values. Figure 9 shows this explicitly in a comparison of the two spectra at 890.7 GHz. The fundamental resonance in the perpendicular mode is reduced by an order of magnitude compared to the parallel-polarization case. The $n=2$ subharmonic appears with roughly comparable amplitude in the two traces.

This amplitude dependence on polarization is most readily understood from the point of view of the local limit $R/\delta\ll 1$ that was considered in the earlier work of Smith, Hebel, and Buchsbaum.[6] These authors have shown explicitly that for the case of a single isotropic system of carriers, and with rf currents directed perpendicular to the field, no CR occurs because of Hall-field screening effects. The net electric field seen by the carriers is the vector sum of the applied linearly polarized field and a Hall field at right angles to it and 90° out of phase with it. This elliptically polarized self-consistent field rotates in a sense opposite to the carrier motion and no energy is absorbed by the carriers at CR. As shown in Ref. 6, various new kinds of resonance modes such as

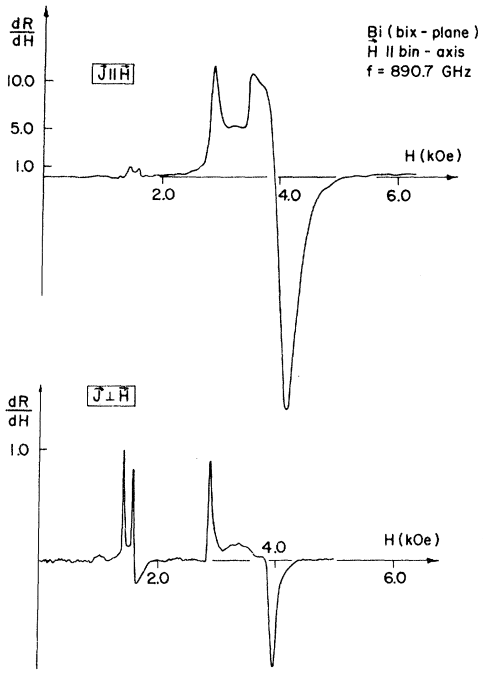

FIG. 9. Comparison of high-frequency CR curves (890.7 GHz) for parallel and perpendicular polarization of the current. The scale marked on the dR/dH axis in arbitrary units gives a measure of the relative amplitude of the two spectra.

hybrid resonance and dielectric anomalies are expected instead of CR. If the rf field is applied parallel to the magnetic field, the Hall effect vanishes and the screening of CR does not apply. For the tilted orbit that we encounter in the Bi resonance, the signal is retained even in the strictly local limit $R/\delta \to 0$, as was recognized in Ref. 6. This is also evident from our Eq. (11), where R/δ appears raised to the power $2n-2$. The fundamental resonance ($n=1$) remains in the limit where R/δ tends to zero.

Our earlier experiments had made use solely of perpendicular polarization, and the observed small amplitude of the fundamental, as well as the fact that it did not scale according to Eq. (11), proved puzzling. With the addition of the parallel-mode data this question has now been resolved.

C. Cyclotron-Wave Effects

As the final point in our discussion of the electrodynamics of high-frequency CR we turn to the consideration of the surface-impedance structure not due to CR transitions. Primarily, these are the pronounced dR/dH minima apparent in Figs. 4–9.

These additional features are, we believe, due to CW of the type first explored by Walsh and Platzman in the alkali metals,[19] and subsequently also observed in Bi by Edelman.[2] The samples used in our experiments are much thicker than characteristic cyclotron wavelengths and they are not in the form of plane-parallel slabs, so that observation of the standing-wave resonances as in Refs. 2 and 19 is precluded in our case. Instead we find structure in the infinite sample impedance due to critical points of the dispersion relation for CW. This is analogous to Henningsen's[20] observations for Ag.

We do not have available calculations of the dispersion relation for CW in Bi that would apply in our range of frequencies. Since CR transitions involve quantum levels with very low index numbers, such calculations should be done quantum mechanically and also should take account of the nonparabolicity of the electronic band structure of Bi. We give a qualitative account of the observed effects based on a hypothetical characteristic dispersion curve as it appears in Fig. 10. This curve gives qR_c vs ω_c/ω for CW with wave vector q for an assumed value of $\omega\tau$ and some particular FS geometry. Our hypothetical curve is similar to those calculated for Ag by Henningsen or for the alkali metals by Foo.[21] As usual, this curve represents the solution to the equation

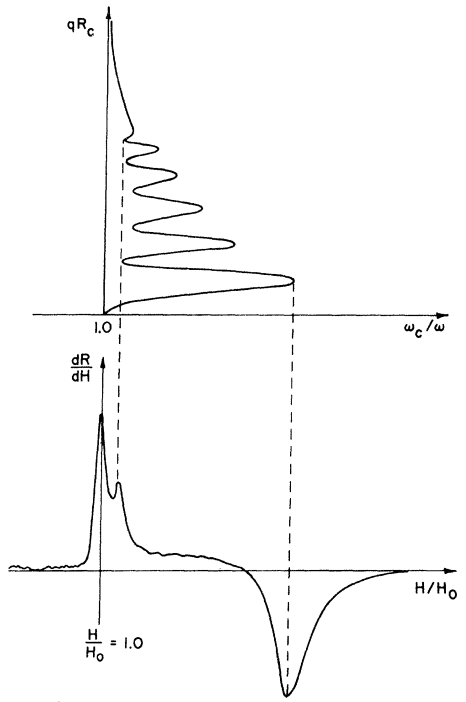

FIG. 10. Hypothetical CW dispersion curve (qR_c vs ω_c/ω) and the related dR/dH curve. The dR/dH curve is observed at 1539.5 GHz. The large negative dR/dH signal corresponds to the cutting off of CW propagation. Structure between the cyclotron resonance at $H=H_0$ and the cutoff field is thought to be due to inner turning points of the dispersion curve.

$$q^2 = (4\pi\omega/c^2)\,\mathrm{Im}\sigma(q, H, \omega)\ . \qquad (12)$$

Propagating waves require in addition that the $\mathrm{Re}\sigma(q, H, \omega)$ and the related damping not be too large. In Fig. 10 only the CW mode related to the fundamental CR has been sketched. Wave propagation commences at the resonance field H_c where $\mathrm{Im}\sigma$ undergoes a change of sign, and it extends to some field value above CR as dictated by the turning point of the dispersion equation in the vicinity of $qR_c \approx \pi$.

It is easy to qualitatively relate features of the experimental traces, such as Fig. 7, to the dispersion curve. We have done so in Fig. 10. In general, the surface impedance is given by the Fourier integral

$$Z \propto \int_0^\infty \frac{dq}{q^2 - (i\omega 4\pi/c^2)\sigma(q, \omega, H)}\ . \qquad (13)$$

The denominator in the integral is closely related to the wave-dispersion equation, except for the fact that both real and imaginary parts of σ enter in the impedance integral. We observe wave effects strongly, which suggests that $\mathrm{Im}\sigma > \mathrm{Re}\sigma$. In that limit we can think of the impedance integral as a line integral on the dispersion curve plot in Fig. 10, which extends vertically from $qR_c = 0$ to infinity. In general this integral has a number of poles at the intersections of the integration path with the dispersion curve. We expect impedance anomalies at field values where the integration path becomes tangent to the dispersion curve and the denominator of Eq. (13) remains small for a finite range of q. Thus with increasing magnetic field we first expect a step in Z, or peak in dR/dH, when we reach the CR field H_c. A negative step and derivative dip is expected when the field reaches the value $1.55H_c$, where the turning point $qR_c \approx \pi$ is located and wave propagation is cut off. The peak at $1.05H_c$ in the experimental curve is due to some inner turning point of the dispersion curve.

The large CW effects, observed in our experiments, are due to the small values of R/δ. The important Fourier components in the impedance integral center about the value $1/\delta$. In the limit $R/\delta \gg 1$, very large qR values play a predominant role. The geometric oscillations for $qR_c \sim \pi$, 2π, etc., are expected to be of minor significance and lead to weak signals only. This is indeed the case for impedance anomalies as observed in the microwave data on Ag[20] and the alkalis.[21] For Bi and R/δ values on the order of unity we expect to observe a much stronger signal.

In the course of our frequency scaling experiments on the impedance anomalies we have come to observe some features that are not in accord with expectations based on the calculations of Henningsen[20] and Foo.[21] With increasing frequency, the parameter R/δ (sD_0 as used by Henningsen) decreases. By explicit calculation for values $sD_0 = 103$ and 85, and assuming spherical FS geometry, Henningsen[20] has shown that the outer turning point of the dispersion relation moves to a lower value of ω_c/ω, i.e., closer to CR, for increasing frequency. Consequently, the impedance anomaly (the dR/dH minimum) should move closer to CR, contrary to what we observe in Figs. 5–8. The succession of traces show that the cutoff point for wave propagation shifts away from CR with increasing frequency, except for the case of the two HCN frequencies 890.7 and 964.3 GHz. We are unable to explain the unexpected frequency shifts. Possibly the effect of quantization in discrete levels needs to be taken into account—after all, CR at the highest frequency corresponds to an $m = 1$ to $m' = 2$ transition. Also, one may have to consider CW coupled to optical-phonon modes or plasmons in Bi whose frequencies are close to the experimental frequencies.

IV. QUANTUM ASPECTS OF AKCR AND EVALUATION OF BAND PARAMETERS

In the quantum interpretation the nth subharmonic of CR between $k_H = 0$ Landau levels consists of a multiplet of exactly n individual transitions. This follows from the sharply defined occupation statistics at low temperatures and the fact that the nth subharmonic of AKCR requires a transition which changes the level index number by n. In the nonparabolic conduction band of Bi this set of n transitions is nondegenerate, and each subharmonic of CR is found to exhibit a distinct multiplet structure. In an earlier publication[9] we had briefly shown how to interpret this fine structure and how it relates to the parameters of the ellipsoidal nonparabolic (ENP) model[22] of the Bi band structure. On the basis of more extensive data we now present a complete analysis in order to derive the parameters E_g and m_c^* of the ENP model. From the data we also find the value of the Fermi energy E_F.

Much of the experimental data had been introduced in Sec. III. CR transitions appear as sharp positive spikes in the dR/dH traces. In the absence of a detailed theory of the line shapes we mark the resonance field as the position of the maximum dR/dH as one would do in microwave AKCR. Because the line shapes of individual transitions vary (compare, for example, the two peaks at the $n = 2$ subharmonics in Fig. 5), and because of the strong CW effects that accompany the resonance, this line-marking procedure introduces an uncertainty on the order of a fraction of the linewidth. As we have noted in Sec. I, well-defined CR signals were observed only for the low-mass resonances at the binary and bisectrix axes. Later

TABLE II. Experimental and calculated resonance fields; $\vec{H}\|$ binary axis, $T=4.2$ °K, $m_c^*(E_F)\cong 0.0095m_0$.

Frequency (GHz)		890.7	964.3	1539.5	2526.6
H (kOe)	Expt.	2.858[a]	3.365	4.693	7.478
	Calc.	2.856	3.333	4.720	7.512
	$m\rightarrow m'$	$4\rightarrow 5$	$4\rightarrow 5$	$2\rightarrow 3$	$1\rightarrow 2$
H (kOe)	Expt.	1.427[a]	1.485	...	3.725
	Calc.	1.428	1.490	2.360	3.756
	$m\rightarrow m'$	$8\rightarrow 10$	$8\rightarrow 10$	$4\rightarrow 6$	$2\rightarrow 4$
H (kOe)	Expt.	1.576[a]	1.667[a]	...	5.070
	Calc.	1.579	1.666	2.807	4.976
	$m\rightarrow m'$	$9\rightarrow 11$	$9\rightarrow 11$	$5\rightarrow 7$	$3\rightarrow 5$

[a]These four resonances have been used to determine the band parameters E_g and m_c^*.

in this section we show and discuss an example of the binary-axis high-mass resonance. The difficulties encountered in the interpretation of this signal are characteristic of other high-mass signals in various crystallographic directions.

The binary-axis low-mass resonances have been studied over the complete frequency range of our experiments. We have examined these in both trigonal- and bisectrix-plane specimens and with the rf currents both parallel and perpendicular to the applied field. Only very minor differences in peak positions are observed, although resonance amplitudes and line shapes depend considerably on sample plane and current polarization. In Table II the experimental resonance-field values are shown for each of the various subharmonic transitions observed at 890.7, 964.3, 1539.5, and 2526.6 GHz. Where such data were available, the quoted field value is averaged over different sample planes and polarizations. The data at the two HCN frequencies 890.7 and 964.3 GHz are the most complete and best-resolved data and our derivation of the band parameters relies on these. In particular, in the analysis below we have chosen four transitions of these data to find band-parameter values that best fit these in a least-mean-squares sense. We subsequently compute and compare resonance fields for all of the other transitions as in Table II.

The energy levels $E_m(H)$ according to the ENP model are given by

$$E_m(1+E_m/E_g)=(m+\tfrac{1}{2})\hbar\omega_c+\hbar^2k_H^2/2m_H^*\pm\tfrac{1}{2}g\mu_BH\,, \tag{14}$$

where $\omega_c=eH/m_c^*c$, and m_c^* and m_H^* are, respectively, the cyclotron and longitudinal effective masses at the bottom of the conduction band. E_g is the separation between the interacting valence and conduction bands. The very last term in Eq. (14) represents the spin splitting of the Landau levels. It follows from Eq. (14) that the separation of a given pair of Landau levels, say, $E_m(H)-E_{m'}(H)$, is a function of k_H. The level separation is maximal at $k_H=0$ and, just as in the case of AKCR on an anisotropic FS, the resonance will be dominated by transitions in the vicinity of the central section of the FS ellipsoids of Bi. Furthermore, with the magnetic field directed along binary or bisectrix direction, it has been shown that $g\approx 2(m_0/m_c^*)$,[23] so that by choosing the negative sign of the spin term we may simplify Eq. (14) to read

$$E_m(1+E_m/E_g)=m\hbar\omega_c \tag{15}$$

for the $k_H=0$ transitions. Solving for the energy levels, we find

$$E_m(H,\,k_H=0)=-\tfrac{1}{2}E_g+(\tfrac{1}{4}E_g^2+E_gm\hbar\omega_c)^{1/2}\,. \tag{16}$$

From quoted values for E_g and m_c^* it is clear that the term E_g^2 under the radical is small compared to the second term. Neglecting the $\frac{1}{4}E_g^2$ term it can be shown that the fractional splitting of a pair of adjacent lines in a given subharmonic of the binary axis or bisectrix CR is approximately given by

$$\Delta H/H\approx 1/m\,,\quad m\gg 1 \tag{17}$$

where m is the Landau-level index number at E_F. From the knowledge that $m\approx 10$ in a field of 1500 Oe, it follows that the splitting of the two lines in the $n=2$ subharmonic should be on the order of 10% as is indeed observed.

To derive values of E_g and m_c^* we insist that Eq. (16), together with the resonance condition $E_m(H)-E_{m'}(H)=\hbar\omega$, correctly describe field positions of the two second subharmonics and the fundamental at 890.7 GHz, as well as the strong second subharmonic peak at 964.3 GHz. The analysis proceeds by assuming a value of E_g in the range 2–20 meV, then computing the four values of m_c^* necessary to fit each of the four transitions. The correct E_g should produce a unique m_c^* that would fit all four peaks simultaneously. We form the quantity

$$\sum_{i=1}^{4}\frac{(m_{c,i}^*-\langle m_c^*\rangle)^2}{\langle m_c^{*2}\rangle}$$

where $\langle m_c^*\rangle$ is the average of the four values $m_{c,i}^*$, and plot it vs E_g as in Fig. 11. The resultant plot shows a minimum near the value $E_g=13.0$ meV for which $m_c^*=0.00170m_0$. The finite value of this minimum is most likely due to experimental errors in the resonance-field determination.

Using $E_g=13.0$ meV and $m_c^*=0.00170m_0$, we next compute field positions for each of the other resonances listed in Table II. In each case, theory and experiment agree to within a fraction of the resonance linewidth so that we conclude that the band parameters, chosen on the basis of four particular peaks, fit the other resonances equally

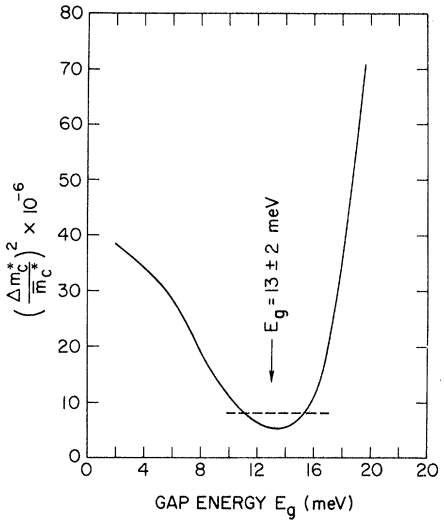

FIG. 11. Mean-square deviation of the cyclotron masses vs assumed gap energy E_g.

well.

We next show how to determine the electronic parameters E_F and the cyclotron mass at the Fermi level $m_c^*(E_F)$ from our data. Toward this end we exhibit the quantum transitions at $k_H = 0$ as shown in Fig. 12. Here the energy levels as given by Eq. (16) are plotted versus magnetic field for the optimum set of band parameters determined earlier. The set of observed transitions for 890.7 GHz (3.684 meV) are drawn at the experimental field values. It is expected that the strength of a given transition will depend on the density of states for each of the Landau levels, the size of the matrix element which expresses the coupling of the electron wave functions to the electric field, and finally the statistical occupation factors $f(E)$ for initial and final states. By comparing a pair of adjacent transitions, such as 8 – 10 and 9 – 11, within the same subharmonic we ensure that the density of states and the transition matrix elements will be nearly the same. Differences in the amplitudes of the resonances within a subharmonic will then be determined by the occupation factors. The Fermi factor $f(E_m) = (1 + e^{(E_m - E_F)/kT})^{-1}$ is dependent on the position of E_m relative to the Fermi level E_F and on temperature. By measuring the amplitudes of peaks within a given multiplet as a function of temperature it is therefore possible to obtain the Fermi energy. In Fig. 13 we show how the pair of peaks of the $n = 2$ subharmonic at 964.3 GHz changes with increasing temperature. We interpret the observed amplitude ratio of the two peaks according to the product of Fermi factors $f(E_m)\,[1 - f(E_m')]$. The value of E_F is chosen for a best fit to the observed amplitudes. Thus we assume that the CR transition from the m to m' level has a strength proportional to the probability that level m be occupied, $f(E_m)$, and that the upper state m' be empty, i.e., $1 - f(E_m')$. In Fig. 14 the amplitude ratios are plotted as a function of temperature and compared with the variation of $f(1 - f)$ for different values of E_F. We do this for the pair of second subharmonic peaks at each of the two HCN frequencies. A best fit for the 890.7-GHz data requires $E_F = 29.45$. At 964.3 GHz we are led to the value $E_F = 29.9$ meV. Amplitudes have been read as the height of the dR/dH peak above the background on the low-field side of the peak. We believe that the different E_F values result from the overly simplified description of resonance amplitude as proportional to $f(1 - f)$. For a more detailed analysis a better theoretical interpretation of resonance line shape and amplitude are necessary. Nevertheless, the sensitive dependence of relative amplitudes on the value of E_F convinces us that a value of $E_F = 29.7$

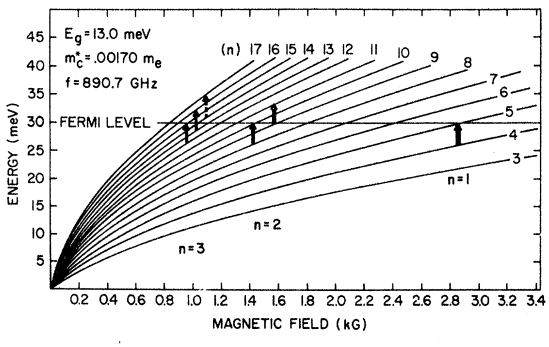

FIG. 12. Landau-level energies vs applied magnetic field. Resonance transitons for 890.7 GHz are indicated by the arrows. The third transition of the $n = 3$ triplet of peaks (broken arrow) is observed weakly at finite temperatures.

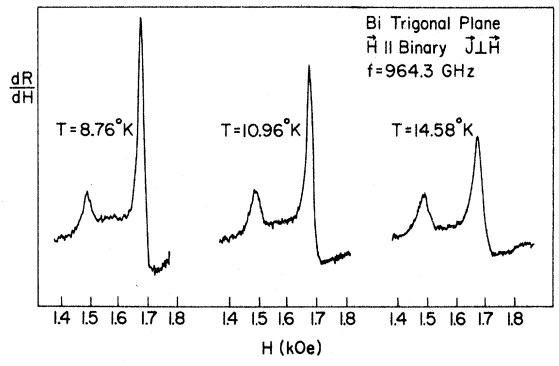

FIG. 13. Variation of the relative peak amplitude with temperature for the doublet of lines at the second subharmonic of the 964.3-GHz resonance. At 4.2 °K the first of the two peaks is barely evident (compare the insert in Fig. 6).

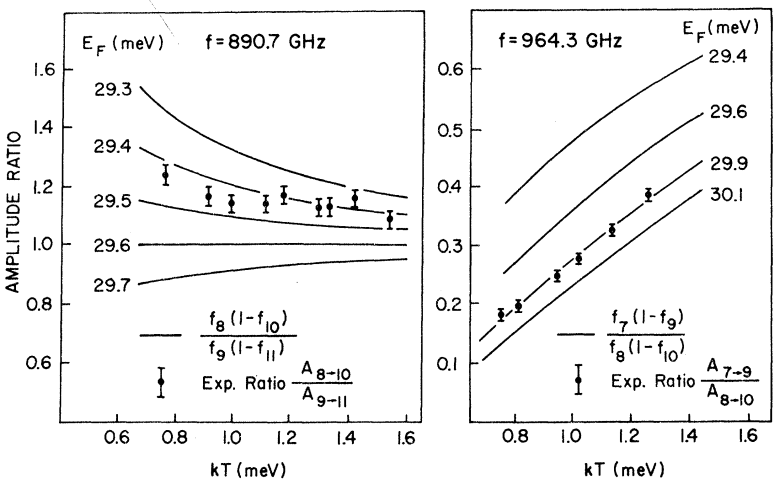

FIG. 14. Peak amplitude ratios for the second subharmonics at 890.7 and 964.3 GHz vs temperature. The experimental points are compared with several curves (solid lines) computed from the ratio of Fermi factors for different assumed values of the Fermi energy E_F.

meV, as obtained from the average of the two curves in Fig. 14, should be correct to ± 0.5 meV when used in conjunction with the band parameters $E_g = 13.0$ meV and $m_c^* = 0.00170 m_0$.

It is also possible that the neglect of the $k_H \neq 0$ transitions can introduce some error in our E_F determination. To illustrate the effect of the $k_H \neq 0$ transitions we take, for example, the $8 \rightarrow 10$ transition which occurs at 1430 Oe for $k_H = 0$ at 890.7 GHz. For finite k_H a larger magnetic field value is required for resonance. The finite linewidth of about 20 Oe for this resonance implies, as we have estimated, that electrons within a band with a width of about 10% of the length of the ellipsoid contribute to the resonance. Thus transitions, as sketched in Fig. 1, do not just occur at $k_H = 0$ but extend over about 10% of the ellipsoid length from $k_H = 0$. There are also a few additional transitions from other sets of Landau levels and other values of k_H, but these can be neglected. The spread of k_H values for contributing electrons also means a spread in $E_m(k_H)$ and $E'_m(k_H)$, rising by about 0.5 meV at the end of the 10% zone for the chosen example. Within this zone the parabolic variation of the energy-level separation will weight most strongly the electrons near $k_H = 0$. Thus the average increase of the energy level due to $k_H \neq 0$ contributions will be only a fraction of 0.5 meV, say, on the order of 0.2 meV. Such considerations help explain the discrepancy in the E_F values determined from amplitude plots and makes the error estimate of ± 0.5 meV for E_F reasonable.

A remark about the assumption $g = 2(m_0/m_c^*)$, and consequent neglect of all spin effects in the foregoing discussion, is in order. According to Ref. 23, the g factor should be $g = 2(m_0/m_s^*)$, with the spin effective mass m_s^* related to m_c^* as $m_c^* = 1.07 m_s^*$. It is possible to show from Eq. (14) that this would lead to a further fractional splitting of each CR transition by an amount

$$\frac{\Delta H}{H} \approx \frac{1}{2m}\left(1 - \frac{m_s^*}{m_c^*}\right) \approx \frac{3.5\%}{m} , \tag{18}$$

where m is the Landau-level index number at E_F. No such splitting has been observed for any of the resonances, even at the highest frequencies where m is small. The observed linewidths always exceed the expected splitting. The determination of the band parameters is of course unaffected by a symmetric broadening of the line due to spin effects. However, one must exercise some care in relating observed linewidths and electron lifetime effects.

We now compare our values of the band parameters with those of other experiments.[4,23,24] In Table III we quote E_g, m_c^*, and E_F, as well as the cyclotron mass of the Fermi energy $m_c^*(E_F)$, computed from the relation

$$m_c^*(E_F) = (1 + 2E_F/E_g) m_c^* .$$

We also form the quantity

$$\frac{A}{2\pi m_c^*(E_F)} = \frac{1 + E_F/E_g}{1 + 2(E_F/E_g)} E_F ,$$

where A is the appropriate cross-sectional area of the FS in momentum space for $\vec{H} \parallel$ binary axis. The values for A and $m_c^*(E_F)$ have been measured accurately in de Haas–van Alphen and microwave CR experiments, respectively. This particular combination of parameters can also be quoted in the present experiment to considerably greater accuracy than the parameters E_g and E_F separately. With reference to Table III we note that our values of E_g and m_c^* are in reasonable agreement with those of Maltz and Dresselhaus,[4] although the ratios E_g/m_c^* vary by about 7%. The particular choice of E_g in our analysis is not crucial for the determination of the E_F. We find that for values of $E_g = 13 \pm 2$ meV the corresponding range for the Fermi energy is $E_F = 29.7 \pm 0.6$ meV. The value

TABLE III. Comparison of band-parameter values.

Parameter	Present experimental	MD (Ref. 4)	SBR (Ref. 23)	Other
E_g (meV)	13.0 (± 2.0)[a]	11.0	15.3	
m_c^*/m_0[b]	0.00170 ($\pm 0.000\,25$)	0.001 56	0.002 10	
$m_0(E_g/m_c^*)$ (eV)	7.60 (± 0.06)	7.1	7.3	
E_F (meV)	29.8 (± 0.6)	(27.3)[c]	27.6	
$m_c^*(E_F)/m_0$	0.00948 ($\pm 0.000\,01$)		0.0097	0.0093 (Ref. 1)
$\frac{A}{2\pi m_c^*(E_F)} = E_F \frac{1+E_F/E_g}{1+2(E_F/E_g)}$ (meV)	17.57 ∓ 0.06	(15.9)[c]	16.8	17.29[d] 17.71[e]

[a]Quoted uncertainties are due to the range of possible values for E_g ($\pm$ meV). The actual experimental errors at any given E_g are approximately $\pm 1\%$.

[b]All cyclotron masses refer to the case of the small mass for $\vec{H} \parallel$ binary axis.

[c]Values of $E_F = 27.3$ and $A/2\pi m_c^*(E_F) = 15.9$ were obtained from the measured E_g, m_c^*, and an assumed value of $m_c^*(E_F) = 0.0093\ m_0$.

[d]These are values of $A/2\pi m_c^*(E_F)$ calculated from A as measured in Refs. 25(d), 26(e), and $m_c^*(E_F) = 0.0093 m_0$.

for E_F of 27.6 meV due to Smith, Baraff, and Rowell[23] is outside our experimental uncertainty. In careful studies at microwave frequencies Khaikin[1] has measured the cyclotron mass at the Fermi level for $\vec{H} \parallel$ binary axis as $m_c^*(E_F)/m_0 = 0.0093 \pm 0.0001$. Our value of 0.00947 ± 0.0001 is in substantial agreement with this. The quantity

$$\frac{A}{2\pi m_c^*(E_F)} = E_F \frac{1+E_F/E_g}{1+2(E_F/E_g)}$$

is determined in the present experiment to about 1% accuracy. Our values of 15.57 meV compares favorably with values of 17.29 or 17.71 meV based on Khaikin's[1] mass value and the area measurements of Bhargava[25] and Brown.[26] The results of Maltz and Dresselhaus[4] combined with Khaikin's mass value give the quantity $[A/2\pi m_c^*(E_F)](E_F)$ as 15.9 meV. The value due to Smith, Baraff, and Rowell is 16.8 meV. Both 15.9 and 16.8 meV are outside reasonable error limits on the measured values of A and $m_c^*(E_F)$.

The foregoing discussion has concentrated on the binary-axis low-mass resonances as the best example of quantum effects in AKCR. The data consist of a single-resonance series and are not seriously perturbed by propagating wave effects. Data taken along the bisectrix axis as in Fig. 15 are dominated by a dielectric anomaly signal. In the dR/dH trace individual CR transitions for each of two electron masses can be readily identified. A fundamental and two second subharmonic peaks appear for each of the two electron masses. The peaks are fit satisfactorily using the previously determined E_g and the m_c^* value scaled according to the know ratio of the microwave cyclotron masses for binary and bisectrix directions. The dielectric anomaly signal is found to fall between the fundamentals of the high- and low-mass resonances.

The observation and interpretation of individual CR transitions due to the higher masses in Bi is generally made difficult by the many propagating electromagnetic wave modes, hybrid resonances, and dielectric anomalies that occur at high magnetic fields. In particular, along the trigonal direction we have found it impossible to identify the

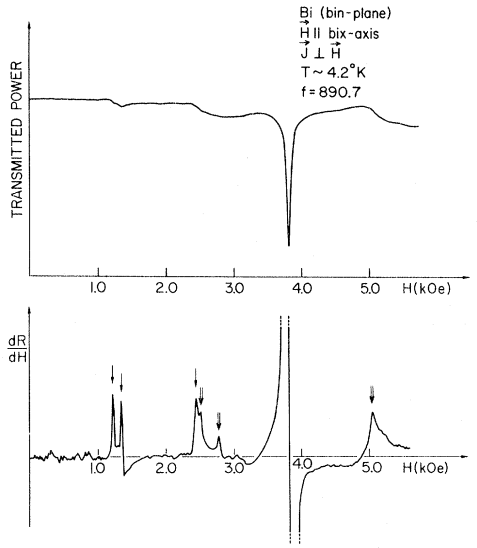

FIG. 15. Transmitted power and dR/dH curves for an orientation within a few degrees of the bisectrix axis. The structure at 3.8 kOe is the dielectric anomaly. CR peaks for two different masses are marked with single and double arrows. The pair of peaks at 2.5 kOe is not resolved when the field is exactly at the bisectrix axis.

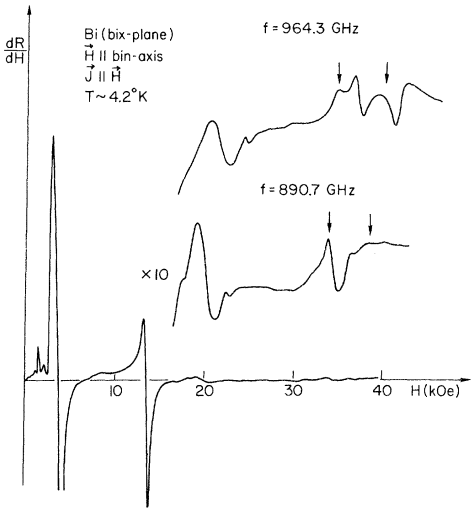

FIG. 16. dR/dH curves for the binary-axis high-mass CR. The positions marked by arrows indicate where the two spin-split fundamental resonances are expected.

many observed peaks and relate them to the known microwave CR signals. Another such case, which exemplifies the difficulties involved in the interpretation of CR, is the high-electron mass $[m_c^*(E_F) = 0.12m_0]$ resonance at the binary axis (Fig. 16). The structures near 35 and 20 kOe are linked with, respectively, the fundamental and second subharmonic transitions of CR. Since the g factor is not close to the value $2(m_0/m_c^*)$, spin-up and spin-down CR transitions are expected to be observed at separate field values. Thus two separate fundamental peaks and four second subharmonic peaks should be observed, each with an amplitude determined by the appropriate Fermi factors. We use the relation $m_c^* = 0.35m_s$ as given in Ref. 23 to calculate the spin-split levels for the high mass. With $E_g = 13.0$ meV, and an m_c^* value adjusted by the known ratio of microwave cyclotron masses, we calculate for 890.7 GHz resonance fields of 33.8 and 38.6 kOe for the spin-split fundamental. These are marked in Fig. 16. Taking into account the lowering of E_F with applied field,[23] the first of these transitions is allowed and possibly corresponds to the peak at 33.9 kOe in the experimental curve. The higher field resonance is probably forbidden by the statistics factor and this may be the reason why no prominent structure can be linked with this transition. At the higher frequency of 964.3 GHz we expect to observe a peak at 34.6 kOe. The second calculated peak at 39.6 kOe would probably be forbidden by the occupation statistics. Both are marked in the figure. It is evident that the marked positions do not explain the observed structures satisfactorily. The situation is even worse with regard to the subharmonic resonance near 20 kOe where no individual CR transitions can be identified. We have examined this resonance also with currents directed perpendicular to the field (for 0–20 kOe) without substantially different results. We believe that the signals we observe at the subharmonic position are not strictly CR but, as in the work of Nakahara *et al.*,[27] represent impedance structure due to the influence of CR on a propagating-wave mode. According to the work of Smith, Hebel, and Buchsbaum[6] we expect that the structure at 35–40 kOe also contains a hybrid resonance.

V. ELECTRONIC LIFETIME EFFECTS IN HIGH-FREQUENCY CYCLOTRON RESONANCE

Recent studies of high-frequency CR in Pb, Hg, and In[5] have shown a frequency-dependent increase in electron scattering with increasing frequency in the range 70–450 GHz. Such effects are expected due to the electron-phonon interaction and its dependence on the energy of the electronic state with respect to the Fermi level.

A similarly increased relaxation rate is apparent from the resonance linewidths of our data on Bi. At the microwave frequency 32 GHz we have judged our samples to have $\omega\tau \approx 40$, and the relative linewidth $\Delta H/H$ is about 4%. We would expect an $\omega\tau$ of 1200 at 960 GHz and a linewidth of about 0.13% assuming that the latter would scale as in the usual CR experiment. We observe a line at least one order of magnitude wider than this, and thus have evidence for increased scattering with higher frequency. An increase in the scattering rate has previously been reported for Bi at 890.7 GHz from a study of the dielectric anomaly,[14] and in the frequency range 10–135 GHz from CR measurements.[28]

One special feature of the quantum CR in Bi, and the selection of $k_H = 0$ transitions because of nonparabolicity, is that the energy separation $E_m - E_F$ is well defined for each of the levels that participate in the resonance. Our experiment probes electron scattering and the effective mass at the distinct energies of the final and initial states. In contrast, the dielectric anomaly measurement averages over electron states distributed smoothly about the Fermi energy.

We present some data on the temperature-dependent linewidths of CR as observed in the present experiments. Shown in Fig. 17 are the results for three particular transitions, each situated differently with respect to the Fermi level as shown in the lower right-hand corner of the figure. The halfwidth ΔH is taken as the width of the positive part of the dR/dH resonance peak at half-maximum. The data are expressed in terms of the quantity $(\Delta H/H)\omega$, which is expected to be propor-

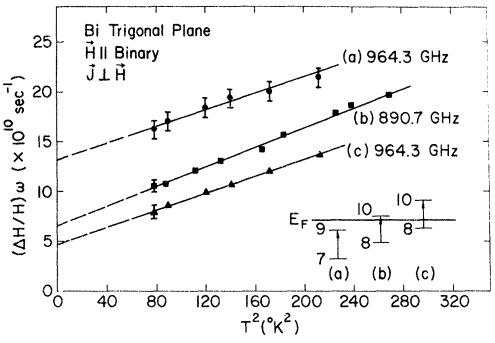

FIG. 17. CR linewidth parameter $[(\Delta H/H)\omega]$ vs T^2 for three resonances located at different energies relative to the Fermi energy.

tional to the scattering rate γ. The data range from 8–17 °K and are seen to follow a T^2 dependence within experimental error. Such a dependence on temperature is characteristic of Bi and is observed in a number of experiments. Previous measurements of the dielectric anomaly at 890.7 GHz [14] have found that the scattering rate could be expressed in the form

$$\gamma(\omega, T) = 1/\tau + \gamma(\omega) + BT^2 . \quad (19)$$

Our CR linewidths agree qualitatively with the predictions of Eq. (19), if one interprets the different $T=0$ intercepts in Fig. 17 as a measure of the dependence of scattering on the position of the resonant Landau levels with respect to E_F. Thus $\gamma(\omega)$ is to be replaced by a term which is a function of $E_m - E_F$ and $E_n - E_F$. This result supports the model of an energy-dependent scattering rate.

To carry our analysis any further requires a theory of the resonance line shape which would allow us to link the measured linewidth $\Delta H/H$ to a relaxation rate γ. It would also be necessary to account for the unresolved spin splitting of CR that is due to the fact that g is only approximately equal to $2(m_0/m_c^*)$. We note that the slope of the T^2 dependence as in Fig. 17 is 4.3×10^8 sec^{-1} °K^{-2}. The work in Ref. 14 determined the coefficient B in Eq. (19) as $B=2.3\times10^8$ sec^{-1} °K^{-2}. Thus if $\Delta H/H$ were related to the scattering time τ as $\Delta H/H \approx 2/\omega\tau$, [29] these slopes would be substantially in agreement.

VI. CONCLUDING REMARKS

We have been able to successfully explain and account for most of the characteristic features of the high-frequency CR data in Bi. These included the multiplet structure of the subharmonics, their amplitude dependence on temperature, the amplitude decay due to relaxation, and finally the CW structures that appear along with the resonances. In review, we want to remind the reader of the outstanding problems. The impedance anomalies due to CW have only been explained in a qualitative way. The location of the anomalies relative to CR, and in particular their frequency dependence, are as yet not accounted for. Because we lack a satisfactory theory of the CR line shapes, neither the resonance position nor electron lifetime have been determined to the accuracy warranted by the experimental uncertainties. This is particularly true for the lifetime effects. We have only been able to indicate that there appears to be an energy dependence of the scattering rate, without being able to determine its functional dependence or magnitude.

Throughout the text we have stressed the fundamental and second subharmonics of CR. The rapid decay of resonance amplitude makes the observation of higher-order subharmonics difficult. The $n=3$, 4 subharmonics can be resolved with increased sensitivity of the spectrometer and we show an example of such data in Fig. 18. Three individual transitions of the $n=3$ peak are resolved, and there would seem to be some fine structure on the $n=4$ resonance as well. As is evident, however, from the trace, these high-order subharmonics are masked by the resonance signal due to transitions between magnetic-field-induced surface-electron levels. Such resonances between surface Landau levels have been studied in Bi at microwave frequencies by Khaikin [30] and Koch and Jensen. [3]

Note added in proof. The general discussion regarding the cyclotron waves in Sec. III C and the corresponding Fig. 10 are not correct for the particular case of Bi. Because the cyclotron resonance is due to a tilted orbit, the conductivity function for $E \parallel H$ as in Eq. (9) contains a resonant term of order $(kR)^0$. This leads to a cyclotron-wave spectrum (labeled type I in Ref. 2) whose

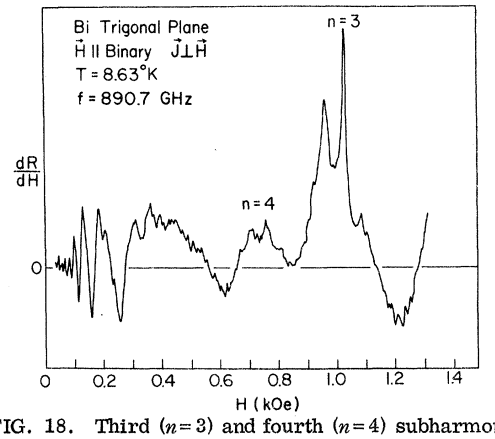

FIG. 18. Third ($n=3$) and fourth ($n=4$) subharmonics for the binary-axis low-mass resonance. Additional resonances in the trace are due to transitions between surface Landau levels.

high-field cutoff is not in the vicinity of $qR_c \approx \pi$, but occurs for $qR_c = 0$. The comparison with the frequency scaling of Henningsen's Ag data, or of the K work by Walsh and co-workers, is not justified. The cutoff for CW propagation is associated with a dielectric anomaly for which the dielectric constant ϵ is equal to 0.

ACKNOWLEDGMENTS

The authors would like to acknowledge the many contributions that H. D. Drew made to the design of the laser spectrometer. He also participated in the early stages of the experiment and provided critical comments and discussion throughout the work. We gratefully acknowledge the many stimulating discussions with J. O. Henningsen regarding the retardation effect and cyclotron waves, as well as his contributions to the construction and operation of our laser spectrometer.

*Present address: Naval Research Laboratory, Washington, D. C. 20375.

[1]V. S. Edelman and M. S. Khaikin, Zh. Eksp. Teor. Fiz. **49**, 107 (1965) [Sov. Phys.-JETP **22**, 77 (1966)].

[2]V. S. Edelman, Zh. Eksp. Teor. Fiz. Pis'ma Red. **9**, 302 (1969) [JETP Lett. **9**, 177 (1969)].

[3]M. S. Khaikin and V. S. Edelman, Zh. Eksp. Teor. Fiz. **47**, 878 (1964) [Sov. Phys.-JETP **20**, 587 (1965)].

[4]M. Maltz and M. S. Dresselhaus, Phys. Rev. B **2**, 2877 (1970).

[5]P. Goy and B. Castaing, in Proceedings of the Thirteenth International Conference on Low-Temperature Physics, Boulder, Colo., 1972 (unpublished).

[6]G. E. Smith, L. C. Hebel, and S. J. Buchsbaum, Phys. Rev. **129**, 156 (1963).

[7]S. J. Allen, Jr., L. W. Rupp, Jr., and P. H. Schmidt, Phys. Rev. (to be published).

[8]H. D. Drew and A. J. Sievers, Phys. Rev. Lett. **19**, 697 (1967).

[9]U. Strom, H. D. Drew, and J. F. Koch, Phys. Rev. Lett. **26**, 1110 (1971).

[10]G. E. Smith, Phys. Rev. **115**, 1561 (1959).

[11]M. Ya. Azbél and E. A. Kaner, J. Phys. Chem. Solids **6**, 113 (1958).

[12]H. D. Drew, Phys. Rev. B **5**, 360 (1970).

[13]A. Kamgar, J. O. Henningsen, and J. F. Koch, Phys. Rev. B **6**, 342 (1972).

[14]H. D. Drew and U. Strom, Phys. Rev. Lett. **25**, 1955 (1970).

[15]B. E. Meierovich, Zh. Eksp. Teor. Fiz. **58**, 1412 (1970) [Sov. Phys.-JETP **31**, 756 (1970)].

[16]R. G. Chambers, Proc. Phys. Soc. Lond. **86**, 305 (1965).

[17]R. E. Prange and Tsu-Wei Nee, Phys. Rev. **168**, 779 (1968).

[18]E. A. Kaner and V. A. Skobov, Adv. Phys. **17**, 605 (1968).

[19]W. M. Walsh, Jr. and P. M. Platzman, Phys. Rev. Lett. **15**, 784 (1965).

[20]J. O. Henningsen, Physics Lab I. Tech University of Denmark, Internal Report No. 77 (unpublished).

[21]P. M. Platzman, W. M. Walsh, Jr., and E-Ni Foo, Phys. Rev. **172**, 689 (1968).

[22]B. Lax and J. G. Mavroids, in *Advances in Solid State Physics*, edited by F. Seitz and D. Turnbull (Academic, New York, 1960), Vol. 11.

[23]G. E. Smith, G. A. Baraff, and J. M. Rowell, Phys. Rev. 135, A1118 (1964).

[24]R. N. Brown, J. G. Mavroides, and B. Lax, Phys. Rev. **129**, 2055 (1963).

[25]R. N. Bhargava, Phys. Rev. **156**, 785 (1967).

[26]R. D. Brown, III, Phys. Rev. B **2**, 928 (1970).

[27]J. Nakahara, H. Kawamura, and Y. Sawada, Phys. Rev. B **3**, 3155 (1971).

[28]S. M. Cheremisin, V. S. Edelman, and M. S. Khaikin, Zh. Eksp. Teor. Fiz. **61**, 1112 (1971) [Sov. Phys.-JETP **34**, 594 (1972)].

[29]For microwave CR in the small-signal limit one finds $\Delta H/H = 1.55/\omega\tau$ for the resonance due to an isotropic mass.

[30]M. S. Khaikin, Zh. Eksp. Teor. Fiz. Pis'ma Red. **4**, 164 (1966) [JETP Lett. **4**, 113 (1966)].

[31]J. F. Koch and J. D. Jensen, Phys. Rev. **184**, 643 (1969).

PHYSICAL REVIEW B VOLUME 7, NUMBER 6 15 MARCH 1973

Thermal Diffuse X-Ray Scattering and the Compressibility of the Interacting Electron Gas

P. M. Platzman
Bell Telephone Laboratories, Murray Hill, New Jersey 07974

N. Tzoar*
City College of The City University of New York, New York, New York, 10031

(Received 26 July 1972)

We make a general analysis of the thermal diffuse scatteri..g of x rays from metals. The difference between this type of scattering and neutron scattering is emphasized. We show how it is possible, by a careful study of the intensity of x-ray thermal diffuse scattering, to experimentally determine the static screening properties of the conduction-electron liquid. At sufficiently low momentum transfers this is equivalent to a measurement of the electron-liquid compressibility.

The inelastic scattering of x rays and neutrons from metals gives information about the various dynamic structure factors of these interesting many-body systems. In fact, workers in this field have always assumed that there is a physically interesting and experimentally accessible regime